nature physics

SUPPLEMENTARY INFORMATION

DOI: 10.1038/NPHYS2688

# Charge noise and spin noise in a semiconductor quantum device

Andreas V. Kuhlmann,[1] Julien Houel,[1] Arne Ludwig,[1,2] Lukas Greuter,[1] Dirk Reuter,[2,3] Andreas D. Wieck,[2] Martino Poggio,[1] and Richard J. Warburton[1]

[1]*Department of Physics, University of Basel, Klingelbergstrasse 82, CH-4056 Basel, Switzerland*

[2]*Lehrstuhl für Angewandte Festkörperphysik, Ruhr-Universität Bochum, D-44780 Bochum, Germany*

[3]*Department Physik, Universität Paderborn, Warburger Strasse 100, D-33098 Paderborn, Germany*

(Dated: June 5, 2013)

In "Charge noise and spin noise in a semiconductor quantum device"[1], the resonance fluorescence (RF) from a single quantum dot (QD) is used to investigate noise inherent to the semiconductor: charge noise and spin noise. We distinguish between charge noise and spin noise via a crucial difference in their optical signatures. We derive noise spectra for both electric and magnetic fields with Monte-Carlo simulations. The noise decreases with increasing frequency, such that, by operating the device at high enough frequencies, we demonstrate the transform-limit for the QD optical linewidth. Here, we explain the details of the experiments, the data processing and the modelling.

DOI: 10.1038/NPHYS2688

# I. RESONANCE FLUORESCENCE ON A SINGLE QUANTUM DOT

## A. The semiconductor quantum device

The quantum device that is used to probe charge noise and spin noise in a semiconductor is a QD sample grown by molecular beam epitaxy. The data presented in the main article[1] were measured on two QDs from different samples: QD1 from sample A and QD2 from sample B. In addition, data are shown from QD3 from sample B and QD4 from sample C in this supplementary information.

The self-assembled QDs are embedded in a Schottky diode[2,3] as shown in Fig. 1 (a). The layer sequence is:

1. *back contact*
   50 nm $n^+$-GaAs, doping level $\sim 1.7 \times 10^{18}\,\mathrm{cm}^{-3}$

2. *tunnelling barrier*
   25 nm i-GaAs

3. *active layer*
   InGaAs QDs (diameter $\sim$ 20 nm, height $\sim$ 5 nm) with centre wavelength 950 nm.

4. *capping layer*
   samples A and B: 150 nm i-GaAs
   sample C: 434.3 nm i-GaAs

5. *blocking barrier*
   samples A and B: 68 periods AlAs/GaAs 3 nm/1 nm
   sample C: 64 periods AlAs/GaAs 3 nm/1 nm

6. *cap*
   10 nm i-GaAs

7. *Schottky gate*
   samples A and C: 3 nm/7 nm Ti/Au
   sample B: 5 nm/10 nm Ti/Au.

Samples A and B only differ in the gate thickness, they are from the same wafer. Sample C is from a different wafer grown under similar conditions with increased capping layer thickness. Our previous spectroscopic

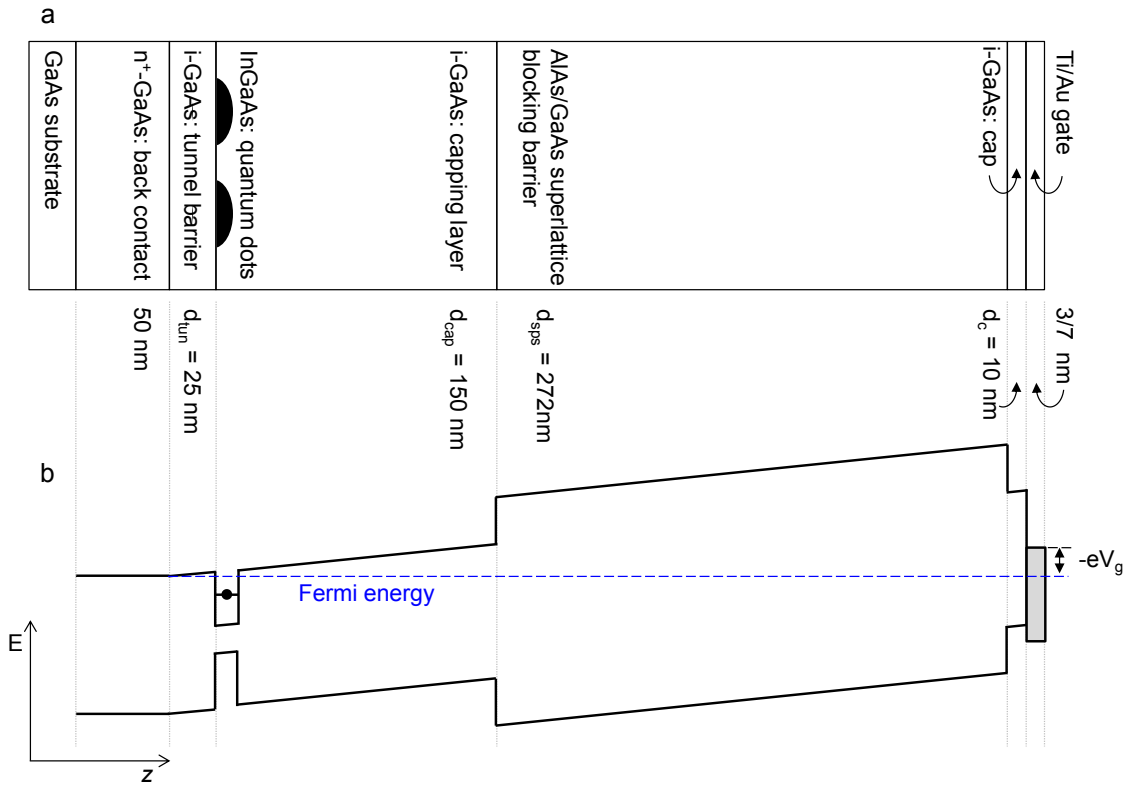


FIG. 1. (a) **Structure of sample A** and the corresponding (b) **Energy band diagram**. The Fermi energy is pinned to the conduction band edge of the back contact. The figures are to scale with respect to length.

experiments[4] showing clear single charging events from holes trapped at the capping layer/blocking barrier interface were carried out on a sample from the same growth system but with 30 nm capping layer thickness.

The background doping of as-grown GaAs is p $\sim 10^{13}\,\mathrm{cm}^{-3}$; two-dimensional electron gases grown under similar conditions have mobilities $> 10^6\,\mathrm{cm}^2/\mathrm{Vs}$.

The number of carriers confined to the QD can be precisely controlled by the gate voltage $V_g$ as illustrated in Fig. 1 (b). A change of gate voltage yields a change of the QD's local potential $\phi$ by

$$\Delta\phi = \frac{\Delta V_g}{\lambda} \tag{1}$$

where $\lambda$ denotes the sample's lever arm, defined as the ratio of back contact to gate distance $d$ and tunnel barrier thickness. For samples A and B $\lambda = 18.3$, for sample C $\lambda = 29.0$, respectively. The exciton energy $E$ is detuned with respect to the constant laser frequency by exploiting the dc Stark effect,

$$\Delta E = a\Delta F, \quad \Delta F = \frac{\Delta V_g}{d} \tag{2}$$

with Stark shift coefficient $a$ and electric field $F$. The Stark shift is determined by recording the resonance position in $V_g$ for many laser frequencies, the laser frequency measured in each case with an ultra-precise

DOI: 10.1038/NPHYS2688

| **Stark shift *a*** ($\mu$eVcm/V) | **QD1** | **QD2** | **QD3** | **QD4** |
|---|---|---|---|---|
| $X^0$ | 0.0324 | 0.0320 | 0.0306 | 0.0377 |
| $X^{1-}$ | 0.0240 | 0.0266 | 0.0219 | 0.0296 |

TABLE I. **Stark shift coefficient of neutral exciton and trion.**

wavemeter. The Stark shift is linear in $\Delta F$ for the small windows of $V_g$ used here, Fig. 5 (b). The neutral exciton $X^0$ has a larger Stark shift than the trion $X^{1-}$ and thus it is more sensitive to charge noise, Table I.

### B. Resonance fluorescence

The quantum dot optical resonance is driven with a resonant continuous-wave laser (1 MHz linewidth) focused on to the sample surface. Reflected or scattered laser light is rejected with a dark field technique using crossed linear polarizations for excitation and detection[5]. The axes of linear polarization are aligned to the sample's crystal axes. The polarization of the neutral exciton is nearly parallel to the crystal axes for QD1, and rotated by $\sim \pi/4$ for QD2, QD3 and QD4. Consequently, at zero magnetic field only the higher energy $X^0$ transition (blue transition) of QD1 is observed in resonance fluorescence (RF), whereas both lower (red transition) and higher energy transitions are observed for the other QDs. The transitions to the trion states are circularly polarized.

The laser power is chosen to lie below the point at which power broadening can be observed, Table II. Resonance fluorescence is detected with a silicon avalanche photodiode in photon counting mode. The arrival time of each photon is recorded over the entire measurement time $T$.

The experiment is not shielded against the earth's magnetic field, thus $B_{\min} \sim 50\,\mu$T. All the experiments were performed with the sample at 4.2 K.

| **noise measurement** | **Fig. 2 (a)** | **Fig. 2 (b)** | **Fig. 4 (a)** |
|---|---|---|---|
| exciton | $X^{1-}$ | $X^{1-}$ | $X^0$ |
| $\Omega/\Gamma_0$ | 0.73 | 0.84 | 0.74 |
| $\Gamma_0$ ($\mu$eV) | 0.75 | 0.74 | 0.93 |

TABLE II. **Laser power**. The Rabi frequency $\Omega$ is stated as a multiple of the transform-limit $\Gamma_0$ for all the noise measurements presented in the main article[1]. $\Gamma_0$ is given with an error of $\pm 0.1\,\mu$eV.

## II. CHARGE NOISE AND SPIN NOISE: EXPERIMENTS

### A. Determination of quantum dot noise spectrum

Post measurement, a binning time $t_{\rm bin}$ is selected, typically $1\,\mu$s. The number of counts in each time bin is $S(t)$, the average number of counts per bin $\langle S(t)\rangle$. The fast Fourier transform of the normalized RF signal $S(t)/\langle S(t)\rangle$ is calculated to yield a spectrum of the noise power $N_{\rm RF}(f)$, specifically

$$N_{\rm RF}(f) = \left|{\rm FFT}\left[S(t)/\langle S(t)\rangle\right]\right|^2 (t_{\rm bin})^2/T. \tag{3}$$

$N_{\rm RF}(f)$ has the same spectrum independent of the choice of $t_{\rm bin}$ and $T$: smaller values of $t_{\rm bin}$ allow $N_{\rm RF}(f)$ to be determined to higher values of frequency $f$; larger values of $T$ allow $N_{\rm RF}(f)$ to be determined with higher resolution. The high frequency limit of our experiment is only limited by the photon flux. The typical binning time of $1\,\mu$s is not the smallest possible. Smaller values of $t_{\rm bin}$ will however increase the Fourier transform computation time.

All Fourier transforms are normalized[6] such that the integral of the noise power $N_x(f)$ over all positive frequencies equals the variance of the fluctuations $\delta x$,

$$\langle(\delta x)^2\rangle = \int_0^\infty df N_x(f). \tag{4}$$

To record a noise spectrum of the experiment alone, the QD is detuned by $> 100$ linewidths relative to the laser and one polarizer is rotated by a small angle to open slightly the detection channel for reflected laser light, choosing the rotation so that the detected laser light gives a count rate similar to the QD RF. A noise spectrum of the reflected laser light (Fig. 2 (a)) is recorded using exactly the routine used to analyse the RF, yielding $N_{\rm exp}(f)$. $N_{\rm exp}(f)$ has a $1/f^2$-behaviour at low frequencies arising from intensity fluctuations in the setup. For $f > 10$ Hz, $N_{\rm exp}(f)$ has a completely $f$-independent spectrum, $N_{\rm exp} \sim 10^{-5}$ Hz$^{-1}$: this is the shot noise $N_{\rm shot}$. The noise of the experiment is typically larger than the noise of the QD $N_{\rm QD}(f)$. The shot noise is proportional to $\langle S(t)\rangle^{-1}$ (Fig. 2 (b)) and not to $\langle S(t)\rangle^{1/2}$ due to the normalization of $S(t)$ by $\langle S(t)\rangle$ in the calculation of the spectrum. $N_{\rm shot}$ is comparable to $N_{\rm QD}(f)$ at low frequencies ($f \sim 10$ Hz), and exceeds $N_{\rm QD}(f)$ at higher frequencies, Fig. 2 (c).

The noise spectrum of the QD alone is then determined using

$$N_{\rm QD}(f) = N_{\rm RF}(f) - N_{\rm exp}(f). \tag{5}$$

Correction of $N_{\rm RF}(f)$ with $N_{\rm exp}(f)$ where $N_{\rm RF}(f)$ and $N_{\rm exp}(f)$ are not measured simultaneously is successful on account of the high stability of the setup. Furthermore, no spectral resonances in $N_{\rm QD}(f)$ have been discovered. We present here $N_{\rm QD}(f)$ after averaging at each $f$ over a frequency range $\Delta f$ to yield

DOI: 10.1038/NPHYS2688

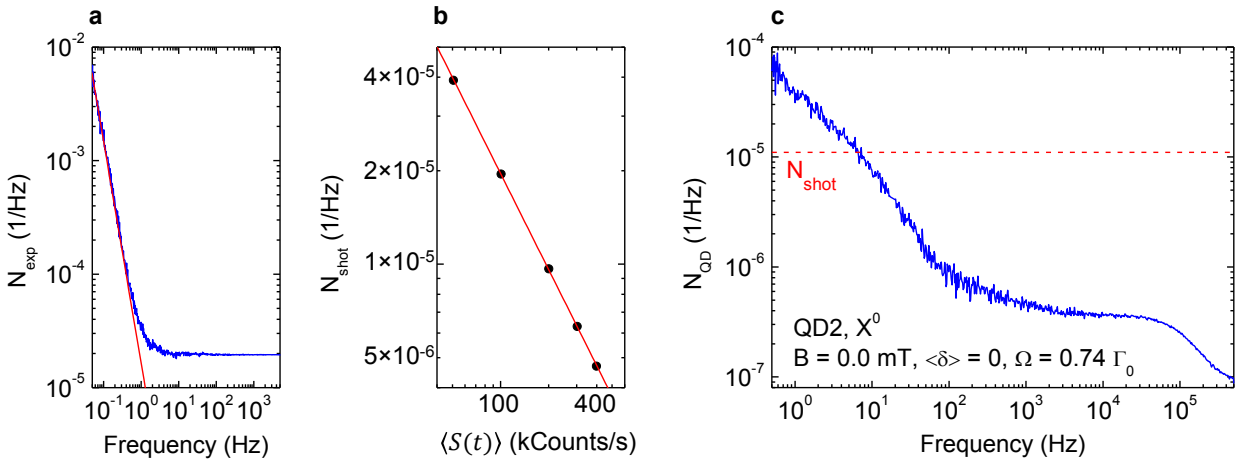


FIG. 2. (a) **Noise spectrum of the experiment**. Intensity fluctuations of the laser cause a $1/f^2$-behaviour of $N_{\rm exp}(f)$ at low frequencies (exponent of red fit $-1.96$). For $f > 10$ Hz the spectrum is dominated by shot noise, thus, the spectrum is flat. The average count rate of the detected laser light is 101 kCounts/s in this particular experiment. (b) **Shot noise**. Noise spectra of the experiment alone were recorded at different laser light count rates to extract the dependence of the shot noise on the count rate. A proportionality of the shot noise to $\langle S(t)\rangle^{-1}$ is verified (exponent of red fit $-1.03$). (c) **Quantum dot noise spectrum**. The noise of the experiment is typically larger than the noise of the QD. The shot noise (red dashed line) typically equals $N_{\rm QD}(f)$ at low frequencies ($f \sim 10$ Hz), and exceeds $N_{\rm QD}(f)$ at higher frequencies. The RF count rate is 176 kCounts/s in this particular experiment. The noise spectrum shown here is the one from Fig. 4 (a) of the main article[1].

equidistant data points on a logarithmic scale. This entire procedure enables us to discern $N_{\rm QD}(f)$ down to values of $10^{-8}$ Hz$^{-1}$ for $T = 2$ hours.

## B. Quantum dot noise

### 1. *Quantum dot-to-Quantum dot dependence*

Noise spectra of three different QDs from the same wafer with 150 nm capping layer – QD1, QD2 and QD3 – are shown in Fig. 3 (a) for the neutral exciton $X^0$ and Fig. 3 (b) for the trion $X^{1-}$, respectively. The $X^0$ noise spectrum of QD2 is presented in Fig. 4 (a) of the main article[1], the $X^{1-}$ noise spectrum of QD2 in Fig. 2 (a) of the main article[1] and the $X^{1-}$ noise spectrum of QD1 in Fig.s 2 (b) and 5 (c) of the main article[1].

For all QDs we find that charge noise is concentrated at low frequencies and that spin noise lies at higher frequencies. For both charge noise and spin noise the quantum dot-to-quantum dot variation of the correlation times is small.

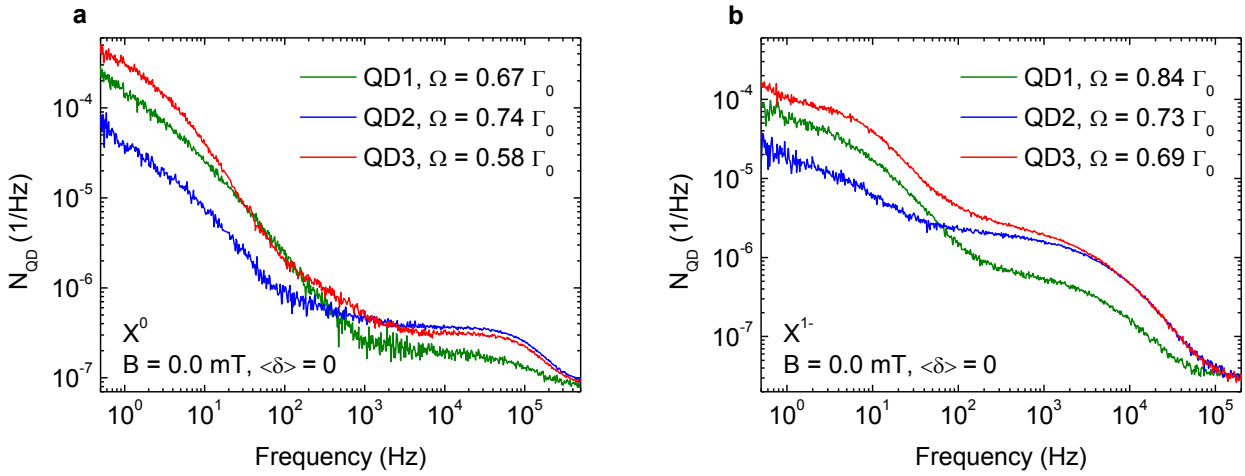


FIG. 3. **Noise spectra of different QDs: neutral exciton $X^0$** (a) **and trion $X^{1-}$** (b). Noise spectra of three different QDs were recorded for both the $X^0$ and $X^{1-}$. The laser power of each measurement is given by the ratio of Rabi energy $\Omega$ to radiative decay rate $\Gamma_0$.

The correlation time of the nuclear spin fluctuations for the neutral exciton $X^0$ is 5.5 $\mu$s for all three QDs. Whereas for QD2 and QD3 the spin noise power is almost the same, QD1 is less sensitive to spin noise, pointing to a smaller electron $g$-factor.

The general behaviour of the charge noise is the same for all QDs, but the charge noise powers are quantum dot dependent. The neutral exciton $X^0$ is more sensitive to charge noise than the trion $X^{1-}$, reflecting the larger Stark shift. In general, the difference in the charge noise power is due either to the different local electrical environment the QD senses or to a difference in sensitivity, on account of the different Stark shifts. QD3 for instance has the smallest Stark shift of all three QDs, Table I, but the largest noise power, i.e. the local electrical environment of QD3 is the noisiest one.

### 2. *Magnetic field dependence*

In Fig. 2 (a) of the main article[1] we present noise spectra of the $X^{1-}$ taken with two detunings, one with average detuning $\langle\delta\rangle = 0$, the other with average detuning half a linewidth, $\langle\delta\rangle = \Gamma/2$. Switching from $\langle\delta\rangle = 0$ to $\langle\delta\rangle = \Gamma/2$ causes the low frequency noise to increase yet the high frequency noise to decrease. This crucial information allows us to distinguish charge noise and spin noise. Sensitivity to charge noise is weak for $\langle\delta\rangle = 0$ yet strong for $\langle\delta\rangle = \Gamma/2$. Spin noise results in a complementary behaviour in the absence of an external magnetic field, $B = 0$.

The identification of charge noise and spin noise can be backed up by experiments in small external magnetic fields. In the presence of an external magnetic field, $B \neq 0$, the trion resonance is split by the

DOI: 10.1038/NPHYS2688

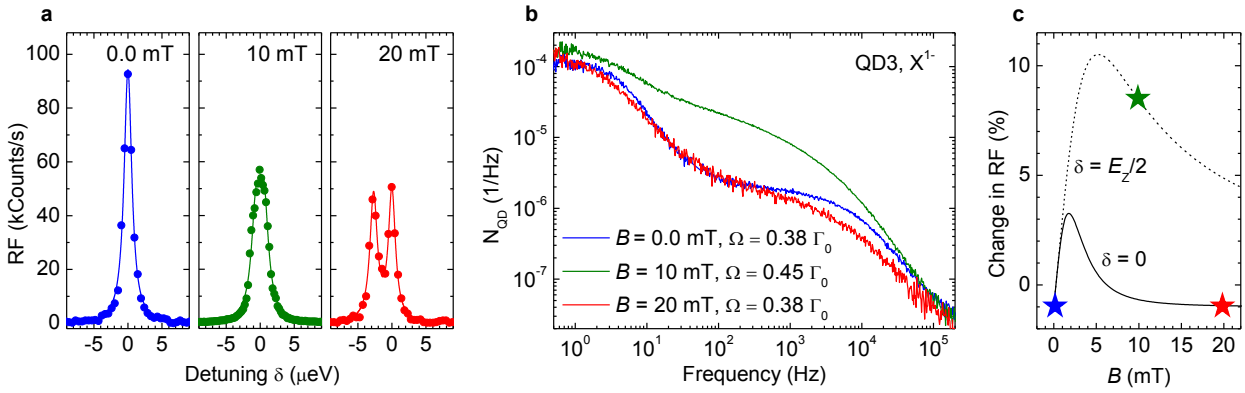


FIG. 4. (a) **RF spectra of the $X^{1-}$ in the presence of a magnetic field**. The trion resonance is split by the exciton Zeeman energy $E_Z$, the splitting is resolved for $B > 10\,\mathrm{mT}$. (b) **Charge noise and spin noise in the presence of a magnetic field**. The corresponding noise measurements. (c) **Simulation of the $X^{1-}$ spin noise sensitivity**. The change in RF for an Overhauser field shift $\Delta\delta = 0.13\,\Gamma_0$, the spin noise sensitivity, is shown for $\langle\delta\rangle = 0$ (solid line) and for $\langle\delta\rangle = E_Z/2$ (dashed line). First the trion's response increases, it then returns to the zero field value remaining constant at higher fields. The colours are used to indicate the same magnetic field, the stars mark the expected value of spin noise sensitivity for the particular measurement.

exciton Zeeman energy $E_Z$. The splitting at low magnetic fields of a few tens of mT is of the order of the linewidth. Resonance fluorescence spectra taken at zero magnetic field and at low fields are shown in Fig. 4 (a). The exciton Zeeman splitting is resolved for $B > 10\,\mathrm{mT}$.

In a small magnetic field we expect charge noise to stay the same yet the trion's response to spin noise first to increase and then to decrease again. Noise spectra of the $X^{1-}$ recorded in a small magnetic field are shown in Fig. 4 (b). Charge noise is unaffected yet spin noise is increased by an order of magnitude at $B = 10\,\mathrm{mT}$ (measured with $\langle\delta\rangle = -E_Z/2$ with respect to the higher energy transition) and returns to the zero field value at $B = 20\,\mathrm{mT}$ (measured with $\langle\delta\rangle = 0$ with respect to the higher energy transition), confirming the expectations on the trion's response to spin noise, Fig. 4 (c).

The external magnetic field affects the nuclear spin dynamics. The higher the field the slower the nuclear spins are. This is already observed for $B$ as small as 20 mT, where the spin noise is shifted to lower frequencies, Fig. 4 (b).

### C. Determination of quantum dot linewidth

In Fig. 2 (c), (d) of the main article[1] the linewidth of the blue transition of the neutral exciton $X^0$ of QD2 is discussed. In addition, we present in Fig. 5 a discussion of the red $X^0$ and the $X^{1-}$ transition of the same QD.

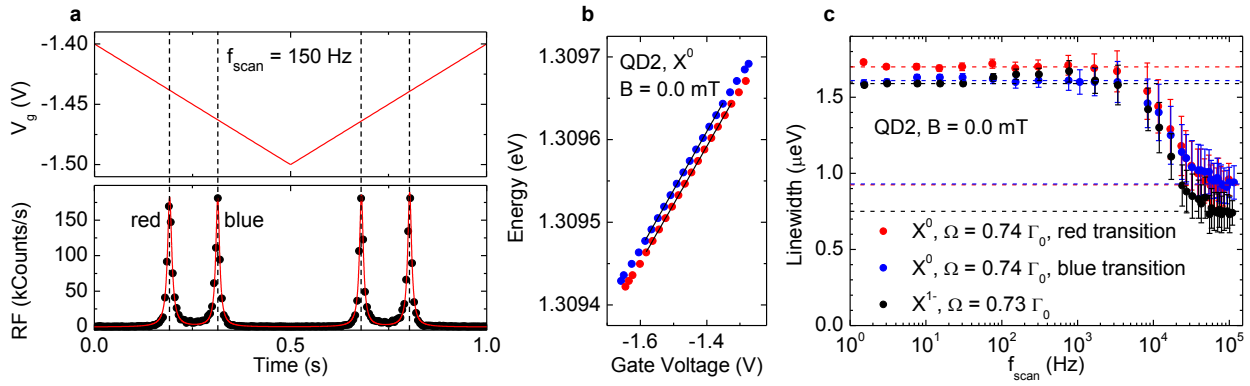


FIG. 5. (a) **Gate voltage and RF time trace**. A triangle voltage signal with 100 mV amplitude and 1 Hz frequency, corresponding to 150 Hz scan frequency, is applied to the gate. The constant laser frequency is set in resonance with the neutral exciton $X^0$. Due to the fine structure splitting of the $X^0$, $\Delta = 17.3\,\mu$eV for QD2, two peaks per scan are observed in the RF even at zero magnetic field. Sweeping to more negative voltages first the lower energy resonance (red) is observed. (b) **Stark shift**. To determine the Stark shift the resonance position in gate voltage is recorded as the laser frequency is varied. The Stark shift for both red and blue $X^0$ transitions is $0.032\pm0.005\,\mu\mathrm{eVcm/mV}$. Solid black lines are linear fits to the data. (c) **Linewidth dependence on scan frequency**. The linewidth for both red and blue transitions of the neutral exciton is recorded as the scan frequency is varied. The constant laser frequency corresponds to the centre of the gate voltage plateau shown in (b). As the scan frequency increases the linewidth decreases from 1.70 $\mu$eV for the red transition and 1.61 $\mu$eV for the blue transition (upper dashed lines) to 0.93 $\mu$eV (lower dashed line) and remains constant at higher frequencies. The radiative lifetime is $0.70 \pm 0.05$ ns ($\Gamma_0 = 0.94 \pm 0.07\ \mu$eV), thus the transform-limit is achieved. The experiment is repeated with the constant laser frequency set in resonance with the $X^{1-}$. The linewidth decreases from 1.59 $\mu$eV to 0.75 $\mu$eV corresponding to the trion's transform-limit of $\Gamma_0 = 0.77 \pm 0.05\ \mu$eV. The mean value of typically 100 Lorentzian fits is plotted as a function of scan frequency; error bars indicate the standard deviation.

To determine the quantum dot optical linewidth $\Gamma$, we apply a triangle voltage signal to the gate with 100 mV amplitude, recording the RF signal as a function of time, Fig. 5 (a). Each time the quantum dot comes into resonance with the constant frequency laser, a peak in the RF is observed. The peak is fitted to a Lorentzian, and the linewidth in mV is converted to a linewidth in $\mu$eV using the known Stark shift.

The linewidth is recorded as the scan frequency is varied, Fig. 5 (c). The scan frequency is defined as the scanning rate divided by the transform-limited linewidth, $f_{\mathrm{scan}} = d\delta/dt/\Gamma_0$ with $\Gamma_0 = \hbar/\tau_r$. For each scan frequency, multiple resonances are recorded and the mean linewidth with error given by standard deviation is plotted as a function of the scan frequency, Fig. 5 (c).

As the scan frequency is increased the linewidth decreases and remains constant at higher frequencies. This constant value corresponds to the transform-limit, determined separately by measuring the exciton lifetime. The radiative lifetime, $\tau_r$, is measured either from an intensity correlation measurement, $g^{(2)}(t)$,

DOI: 10.1038/NPHYS2688

or from a decay curve following pulsed excitation.

## III. CHARGE NOISE AND SPIN NOISE: MODELLING

The experiment determines the spectrum of the noise in the RF and demonstrates that it is dominated by charge noise at low frequency, spin noise at high frequency. The noise sensor, the RF from a single quantum dot, has a trivial dependence on the fluctuating electric $F(t)$ and magnetic fields $B_N(t)$ only for small fluctuations in the detunings around particular values of detuning $\delta$. Monte Carlo simulations allow us to determine both the electric field and magnetic field noise accurately by describing the response of the sensor for all $\delta$, treating charge noise and spin noise on an equal footing.

The basic approach is to calculate $F(t)$ and $B_N(t)$, in each case from an ensemble of independent, but identical, 2-level fluctuators using a Monte Carlo method; to calculate the RF signal $S(t)$ from $F(t)$ and $B_N(t)$; and to compute the noise $N(f)$ from $S(t)$ using exactly the same routine as for the experiments (but without the correction for extrinsic noise of course).

For $X^{1-}$,

$$S(t) = \frac{\frac{1}{2}\left(\frac{\Gamma_0}{2}\right)^2}{(aF(t)+\delta_1(t)+\delta)^2+\left(\frac{\Gamma_0}{2}\right)^2} + \frac{\frac{1}{2}\left(\frac{\Gamma_0}{2}\right)^2}{(aF(t)-\delta_1(t)+\delta)^2+\left(\frac{\Gamma_0}{2}\right)^2}, \quad \delta_1(t) = \frac{1}{2}g\mu_B B_N(t), \quad (6)$$

where $a$ is the dc Stark coefficient and $g$ the electron g-factor.

For $X^0$,

$$S(t) = \frac{\left(\frac{\Gamma_0}{2}\right)^2}{(aF(t)+\delta_0(t)+\delta)^2+\left(\frac{\Gamma_0}{2}\right)^2}, \quad \delta_0(t) = \pm\frac{1}{2}\sqrt{\Delta^2+\delta_1(t)^2}, \quad (7)$$

with $\Delta$ the fine structure splitting. For the blue Zeeman branch $\delta_0(t)$ is positive, for the red one negative, respectively.

An ensemble of identical 2-level fluctuators fully describes spin noise; charge noise is more complex, Fig. 6. The experiment reveals the existence of a dominant 2-level fluctuator that is modelled using a Monte Carlo approach. To fully describe charge noise, post simulation a weak $1/f$-like noise component is introduced.

### A. Spectrum of a 2-level fluctuator

A 2-level fluctuator occupies either state 0 with lifetime $\tau_0$ or state 1 with lifetime $\tau_1$. The probability $p$ of being, at any time, in state 1 is $\tau_1/(\tau_0+\tau_1)$; the probability of being in state 0 is $\tau_0/(\tau_0+\tau_1)$. The

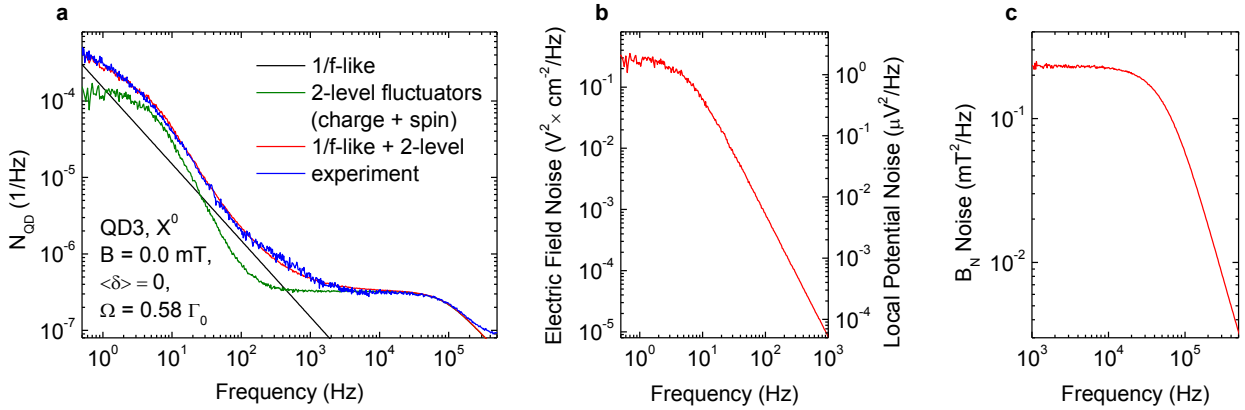


FIG. 6. **Charge noise and spin noise modelling.** Charge noise and spin noise of the neutral exciton $X^0$ of QD3 are calculated from an ensemble of 2-level fluctuators. To fully describe charge noise a $1/f^{\alpha}$ noise component with $\alpha = 1.00$ is added to $N_{\rm QD}(f)$. From the simulations both the electric (without the $1/f$-like noise) and magnetic field noise can be calculated. The rms value for the fluctuations in the local potential is 3.9 $\mu$V corresponding to electric field fluctuations of 1.55 V/cm with a correlation time of 0.03 s. The nuclear spins cause fluctuations of $B_{N,\rm rms} = 145\,\rm mT$ with a correlation time of 5.5 $\mu$s. The parameters used in the simulations are: $N_c = 1.0 \times 10^{10}\,\rm cm^{-2}$, $d = 150\,\rm nm$ and $p = 1.2\%$ for charge noise; $N_{\rm eff} = 115$, $A = 90\,\mu\rm eV$, $g = -0.5$ and $\Delta = 11.5\,\mu\rm eV$ for spin noise.

configuration $C(t)$ of a 2-level fluctuator, either 0 or 1, is determined by the probabilities of a $0 \rightarrow 1$ transition[7],

$$p_{0\rightarrow 1}(\delta t) = 1 - \frac{1}{\tau_0 + \tau_1}\left[\tau_1 \exp\left(-\left(\frac{1}{\tau_0} + \frac{1}{\tau_1}\right)\delta t\right) + \tau_0\right] \tag{8}$$

and a $1 \rightarrow 0$ transition,

$$p_{1\rightarrow 0}(\delta t) = 1 - \frac{1}{\tau_0 + \tau_1}\left[\tau_0 \exp\left(-\left(\frac{1}{\tau_0} + \frac{1}{\tau_1}\right)\delta t\right) + \tau_1\right] \tag{9}$$

where $\delta t$ denotes the time over which the system evolves. The power spectrum of a 2-level fluctuator $S(\omega)$ is Lorentzian[7],

$$S(\omega) = \frac{1}{\pi}\frac{\tau_0\tau_1}{(\tau_0+\tau_1)^2}\frac{1/T}{\omega^2 + (1/T)^2}, \quad 1/T = 1/\tau_0 + 1/\tau_1. \tag{10}$$

### B. Charge noise

The experiment reveals the low frequency noise to be charge noise. There is a Lorentzian power spectrum superimposed on a weak $1/f$-like component in the power spectrum, Fig. 6.

The simulation for the Lorentzian charge noise proceeds by assuming that the noise arises from an ensemble of localization centres, each of which can be occupied by a single hole[4]. Performing the experiments

DOI: 10.1038/NPHYS2688

in Fig. 2 (d) of the main article[1], we very occasionally observe (probability $\sim 2\%$) that the QD resonance shifts by $2.45\,\mu\mathrm{eV}$ from its average position. This is a blue-shift consistent with the trapping of a single hole above the QD. The centres are located at distance $d$ away from the QDs. The energy shift $\Delta E$ of the exciton resonance induced by the electric field $F_{\mathrm{h},z}$ created by a single hole is given by

$$\Delta E = -aF_{\mathrm{h},z}. \tag{11}$$

The approximate in-plane symmetry of the QDs allows only for a significant non zero dipole moment in growth direction $z$. Again, as in the $z$-direction the exciton polarizability can be neglected such that only $F_{\mathrm{h},z}$ contributes to the Stark shift. The electric field $F_{\mathrm{h},z}$ at the position of the QD created by a single positive charge at distance $d$ from the QD, at lateral coordinate $\mathbf{r} = (x, y)$ is given by[4]

$$F_{\mathrm{h},z} = \frac{-e}{4\pi\epsilon_0\epsilon_r}\left[\frac{d}{\left(r^2+d^2\right)^{3/2}} + \frac{d+2d_{\mathrm{tun}}}{\left(r^2+\left(d+2d_{\mathrm{tun}}\right)^2\right)^{3/2}} - \frac{d+2\left(d_{\mathrm{sps}}+d_{\mathrm{c}}\right)}{\left(r^2+\left(d+2\left(d_{\mathrm{sps}}+d_{\mathrm{c}}\right)\right)^2\right)^{3/2}}\right]. \tag{12}$$

Both the hole at distance $d$ and its negative image charges in the metallic back contact and the Schottky gate contribute to the electric field. For example, a hole at distance $d_{\mathrm{cap}} = 150\,\mathrm{nm}$, centred above the QD, shifts the resonance by $+1.65\,\mu\mathrm{eV}$; increased by a negative image charge in the back contact to $+2.57\,\mu\mathrm{eV}$; reduced by a negative image charge in the top gate to $+2.50\,\mu\mathrm{eV}$. The numbers are derived with the neutral exciton's Stark shift of QD3, Table I, and the close agreement with the experimental optical shift of $+2.45\,\mu\mathrm{eV}$ enables us to conclude that $d = d_{\mathrm{cap}}$, i.e. the hole in the environment is located at the capping layer/blocking barrier interface.

To back up this conclusion we measured the noise on a sample with increased capping layer thickness, Fig. 7. For sample C the capping layer thickness was increased from $150\,\mathrm{nm}$ to $434.3\,\mathrm{nm}$ moving the capping layer/blocking barrier interface far away from the QDs. The high frequency noise is unaffected by the increased capping layer thickness, supporting the identification of the high frequency noise to be spin noise. The low frequency noise by contrast changes: the Lorentzian charge noise vanishes and a weak $1/f$-like noise component remains. This strongly supports the assertion that the Lorentzian charge noise is caused by fluctuating holes the capping layer/blocking barrier interface.

We model a two-dimensional array of localization centres. The centres have a density of $N_c$ and, at any particular time, are occupied/unoccupied (states 1/0) with probability $p$, $1-p$ such that the average hole density is $N_h = pN_c$. At $t = 0$, each centre is occupied by a random number generator giving a configuration of localized charges $C(0)$. At a later time, $\delta t$, $C(\delta t)$ is calculated from $C(0)$ again with a random number generator using the probabilities $p_{1\to0}(\delta t)$ and $p_{0\to1}(\delta t)$ from the theory of a two-level fluctuator. The localization centres are treated independently. The localization centres directly above the quantum dot

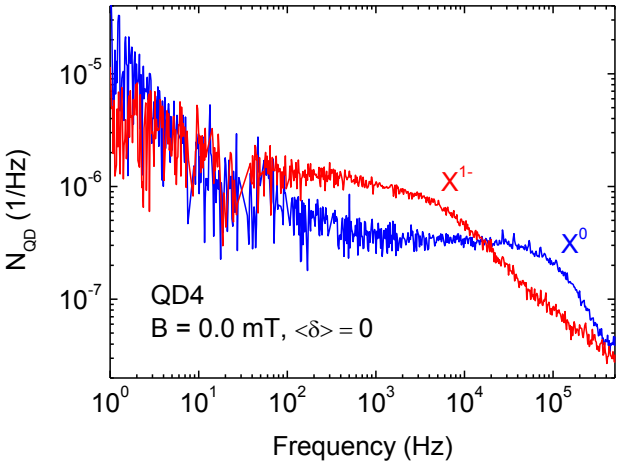


FIG. 7. **Noise dependence on capping layer thickness.** Charge noise and spin noise of both the neutral exciton $X^0$ and the trion $X^{1-}$ for QD4 from sample C with increased capping layer thickness compared to samples A and B.

give rise to substantial energy shifts $\Delta E \sim 2.5\,\mu\mathrm{eV}$ which, as described above, we very rarely observe: we therefore neglect any localization centres in a circle of diameter $0.8\,\mu\mathrm{m}$ about the quantum dot axis. In other words, above-QD localization centres exist, but are occupied with low probability. This is probably related to a strain field above the quantum dot. The procedure is repeated to give $C(0), C(\delta t), C(2\delta t)$, etc. The electric field $F(t)$ is calculated for each $C$.

For the Monte-Carlo simulations charge noise can be controlled by 4 independent parameters: occupation probability $p$, localization centre density $N_c$, distance $d$ and lifetime $\tau_1$ (for $\tau_1 < \tau_0$). Once $p$ and $\tau_1$ are defined, $\tau_0$ cannot be chosen independently: $\tau_1$ is determined by the Lorentzian's linewidth. In principle, a good fit to the experiment can be achieved in a window of $N_c$ and $d$: a high density of far away defects leads to similar charge noise as a lower density of closer defects. In practice however, the occasional rigid shift of $+2.45\,\mu\mathrm{eV}$ and the noise suppression with increased capping layer thickness point strongly to the fact that the localization centres are located at the capping layer/blocking barrier interface. We therefore simulate the Lorentzian charge noise using $d = d_{\mathrm{cap}}$ and $N_c = 1.0 \times 10^{10}\,\mathrm{cm}^{-2}$, a value of $N_c$ we deduced from a sample with $d_{\mathrm{cap}} = 30\,\mathrm{nm}$ for which the spectral shifts on occupying the localization centres are much larger[4].

Post simulation, in $N_{\mathrm{QD}}(f)$ we superimpose the Lorentzian charge noise on a weak $1/f$-like noise component. The power and exponent of the $1/f$-like noise is exciton and also quantum dot dependent and its origin is not known exactly. It is however independent of the power of the resonant laser.

The results of the charge noise simulations for both the neutral exciton $X^0$ and the trion $X^{1-}$ of QD2 are presented in Fig. 8. Both excitons sense the same local electrical environment however with a different Stark shift: the neutral exciton is more sensitive to fluctuations of the electrical environment. A good fit

DOI: 10.1038/NPHYS2688

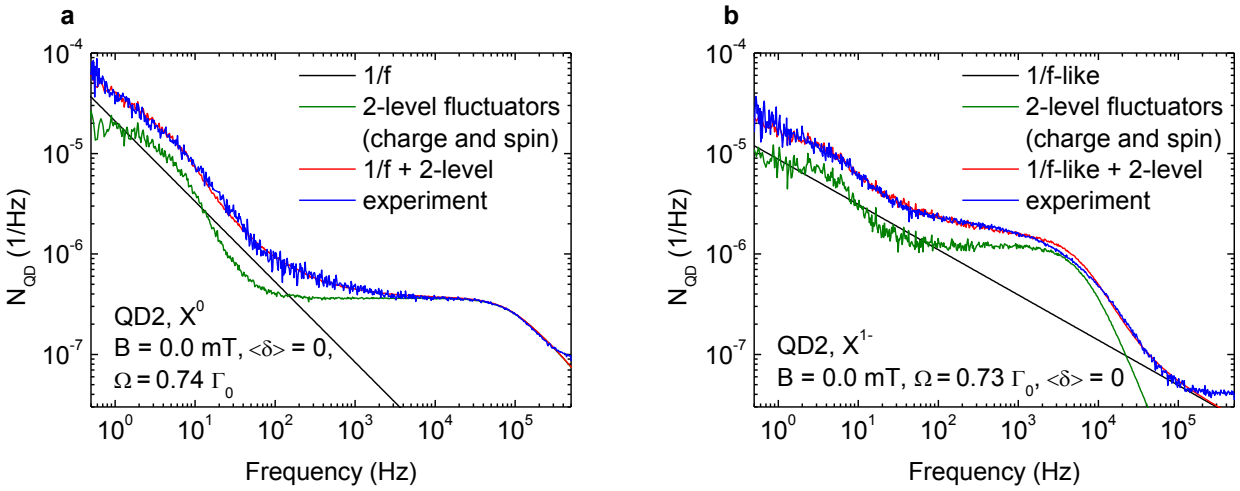


FIG. 8. **Charge noise and spin noise modelling.** Charge noise and spin noise of both the neutral exciton $X^0$ and the trion $X^{1-}$ of QD2 are simulated. Fig. 7 (a) and Fig. 4 (a) of the main article[1] are the same.

to the experiment is achieved for both $X^0$ and $X^{1-}$ by an ensemble of 2-level fluctuators with $\tau_1 = 0.03\,\mathrm{s}$, $N_c = 1.0 \times 10^{10}\,\mathrm{cm}^{-2}$ and $d = 150\,\mathrm{nm}$. The occupation probability $p$ is 0.1 % ($\tau_0 = 30\,\mathrm{s}$) for $X^0$ and 0.46 % ($\tau_0 = 6.5\,\mathrm{s}$) for $X^{1-}$. The difference in $p$ reflects the different charging state of the sample, discussed in section *Sample history* of the main article[1]. The exponent of the superimposed $1/f^\alpha$ noise in $N_{\mathrm{QD}}(f)$ is determined by the slope of $N_{\mathrm{QD}}(f)$ at low frequencies $f \sim 0.1\,\mathrm{Hz}$: $\alpha = 0.8$ for $X^0$, $\alpha = 0.5$ for $X^{1-}$. Note that also the charge noise of QD3 (Fig. 6) can be described with the same local electrical environment as used for QD2.

### C. Spin noise

The calculation of the time trace of the magnetic field $B_N(t)$ proceeds in a similar way, albeit simplified: each nucleus is treated as a two-level fluctuator, with equal $0 \to 1$, $1 \to 0$ transition rates, $1/\tau$. The nuclear magnetic field, the so-called Overhauser field $B_N$, is given by[8]

$$B_N = \frac{v_0}{g\mu_B} \sum_{i=1}^{N} A_i \, |\psi(\mathbf{r}_i)|^2 \, I_i \tag{13}$$

where $v_0$ is the atomic volume, $A_i$ the hyperfine interaction constant, $\mathbf{r}_i$ is the position of the nuclei $i$ with spin $I_i$, and $\psi(\mathbf{r})$ is the normalized electron envelope function. By using an average hyperfine constant[9] $A = 90\,\mu\mathrm{eV}$ and approximating the electron envelope function $\psi(\mathbf{r})$ by a top hat, Eq. (13) simplifies to

$$B_N = \frac{A}{g\mu_B N_{\mathrm{eff}}} \sum_{i=1}^{N_{\mathrm{eff}}} I_i. \tag{14}$$

$N_{\mathrm{eff}}$ denotes the number of nuclear spins inside the top hat envelope function.

Regarding the dimensionality of $B_N$, a 1D model for the nuclear spins is appropriate for both $X^0$ and $X^{1-}$. The isotropic part of the electron-hole exchange interaction "protects" the $X^0$ from the in-plane fluctuations of the nuclear magnetic field. Specifically, the $z$-component of the Overhauser field enters along the diagonals of the exchange/Zeeman Hamiltonian[10] in the $|\Uparrow\downarrow\rangle$, $|\Downarrow\uparrow\rangle$, $|\Uparrow\uparrow\rangle$, $|\Downarrow\downarrow\rangle$ basis and results in the dispersion of Eq. 7. The in-plane components of the Overhauser field couple $|\Uparrow\downarrow\rangle \leftrightarrow |\Uparrow\uparrow\rangle$ and $|\Downarrow\uparrow\rangle \leftrightarrow |\Downarrow\downarrow\rangle$ but these states are split by the dark-bright splitting, 100s of $\mu$eV, determined by the isotropic part of the exchange interaction. As a result the dependence of the exciton energy on the in-plane fields is negligible. For $X^{1-}$, at zero external magnetic field, all three components of the Overhauser field are equally important. However, a simulation of the $X^{1-}$ RF at $B = 0$ gives the same results for a $B_N$ fluctuating in 1D and for a $B_N$ fluctuating in 3D provided $B^{1D}_{N,\mathrm{rms}} = \sqrt{3}B^{3D}_{N,\mathrm{rms}}$. A small $B$ suppresses the sensitivity of $X^{1-}$ to in-plane $B_N$ fluctuations.

We assume that each nuclear spin $I$ can be represented by a spin-$\frac{1}{2}$, a 2-level fluctuator. To account for an underestimate of the hyperfine interaction (the real spins are larger than $\frac{1}{2}$) the Overhauser field is enhanced via a reduction in the total number of nuclei, $N \rightarrow N_{\mathrm{eff}}$. Equivalently, we could work with a higher $N_{\mathrm{eff}}$ and larger $A$. The model represents a phenomenological way to create $B_N(t)$ which mimics the experiment. $B_N(t)$ is unique, the route to $B_N(t)$ is not.

There are two independent parameters that control spin noise in the simulation: the correlation time $\tau$ and the rms field $B_{N,\mathrm{rms}}$. The experiment reveals a smaller nuclear spin correlation time for the $X^0$ exciton than the $X^{1-}$ exciton. Also, the $B_{N,\mathrm{rms}}$ for $X^{1-}$ is lower than that for $X^0$. The origin of the difference is both surprising and not at all obvious. The results of the spin noise simulations for both $X^0$ and $X^{1-}$ of QD2 are shown in Fig. 7. For $X^0$ we extract $\tau = 5.5\,\mu$s and $B_{N,\mathrm{rms}} = 193\,\mathrm{mT}$ ($N_{\mathrm{eff}} = 65$, $A = 90\,\mu$eV, $g = -0.5$, $\Delta = 17.3\,\mu$eV in the simulation), for $X^{1-}$ $\tau = 100\,\mu$s and $B_{N,\mathrm{rms}} = 9\,\mathrm{mT}$ ($N_{\mathrm{eff}} = 310$, $A = 9\,\mu$eV, $g = -0.5$ in the simulation).

The correlation time for the nuclear spin dipole-dipole interaction can be estimated by,

$$\tau = \hbar/E_{dd}, \quad E_{dd} = \mu_{I1}B_{I2} \sim \frac{\mu_0}{2\pi}\frac{\mu_{I1}\mu_{I2}}{d^3}, \quad \mu_i = \hbar\gamma_i I_i \tag{15}$$

with energy $E_{dd}$ of a nuclear dipole with moment $\mu_{I1}$ in the magnetic field $B_{I2}$ of another dipole at distance $d$ and gyromagnetic ratio $\gamma$. For example, taking the average of an In and Ga as one spin and an As spin as the other, separated by the atomic spacing in the GaAs lattice, $\tau = 47\,\mu$s. It gives order-of-magnitude agreement with the correlation time of the spin noise and this allows us to identify the process responsible

DOI: 10.1038/NPHYS2688

for the spin noise: nuclear spin dipole-dipole processes.

---


[1] A. V. Kuhlmann *et al.*, Main article.

[2] H. Drexler *et al.*, Phys. Rev. Lett. **73**, 2252 (1994).

[3] R. J. Warburton *et al.*, Nature **405**, 926 (2000).

[4] J. Houel *et al.*, Phys. Rev. Lett. **108**, 107401 (2012).

[5] A. V. Kuhlmann *et al.*, arXiv:1303.2055.

[6] Sh. Kogan, *Electronic noise and fluctuations in solids*, (Cambridge University Press 1996)

[7] S. Machlup, J. Appl. Phys. **25**, 341 (1954).

[8] B. Urbaszek *et al.*, Rev. Mod. Phys. **85**, 79 (2013).

[9] C. Kloeffel *et al.*, Phys. Rev. Lett. **106**, 046802 (2011).

[10] M. Bayer *et al.*, Phys. Rev. B **65**, 195315 (2002).